THE JOURNAL OF PHYSICAL CHEMISTRY Letters

Letter

Cite This: J. Phys. Chem. Lett. 2018, 9, 4502−4511

pubs.acs.org/JPCL

Impact of the Organic Cation on the Optoelectronic Properties of Formamidinium Lead Triiodide

Christopher L. Davies,[†] Juliane Borchert,[†] Chelsea Q. Xia,[†] Rebecca L. Milot,[†,‡] Hans Kraus,[¶] Michael B. Johnston,*[,†] and Laura M. Herz*[,†]

[†]Department of Physics, University of Oxford, Clarendon Laboratory, Parks Road, Oxford OX1 3PU, United Kingdom

[‡]Department of Physics, University of Warwick, Gibbet Hill Road, Coventry CV4 7AL, United Kingdom

[¶]Department of Physics, University of Oxford, Denys Wilkinson Building, Keble Road, Oxford OX1 3RH, United Kingdom

Supporting Information

ABSTRACT: Metal halide perovskites have proven to be excellent light-harvesting materials in photovoltaic devices whose efficiencies are rapidly improving. Here, we examine the temperature-dependent photon absorption, exciton binding energy, and band gap of $FAPbI_3$ (thin film) and find remarkably different behavior across the $\beta-\gamma$ phase transition compared with $MAPbI_3$. While $MAPbI_3$ has shown abrupt changes in the band gap and exciton binding energy, values for $FAPbI_3$ vary smoothly over a range of 100−160 K in accordance with a more gradual transition. In addition, we find that the charge-carrier mobility in $FAPbI_3$ exhibits a clear $T^{-0.5}$ trend with temperature, in excellent agreement with theoretical predictions that assume electron−phonon interactions to be governed by the Fröhlich mechanism but in contrast to the $T^{-1.5}$ dependence previously observed for $MAPbI_3$. Finally, we directly observe intraexcitonic transitions in $FAPbI_3$ at low temperature, from which we determine a low exciton binding energy of only 5.3 meV at 10 K.

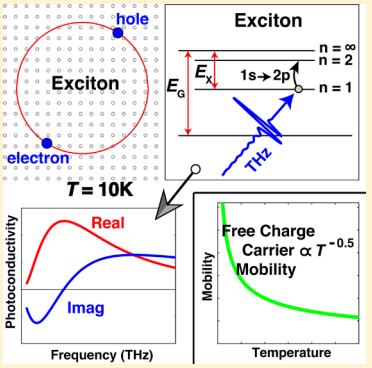

Metal halide perovskites have received an immense amount of interest owing to their potential use as light-absorbing materials in photovoltaic devices. Over recent years, such perovskite solar cells have seen an exciting rise in performance, with current hybrid lead triiodide-based devices achieving efficiencies of over 20%.[1] High charge-carrier mobilities[2−6] combined with long carrier lifetimes[7−11] have been shown to underpin the excellent performance of these materials. In addition, the diversity of deposition techniques, including spin coating,[12,13] vapor deposition,[14−16] and inkjet printing,[17] along with a relatively low cost of fabrication makes metal halide perovskites both economically and also physically favorable for rapid commercialization.

While the wealth of research into metal halide perovskites is rapidly growing, most investigations into the fundamental optoelectronic properties have been focused on the prototypical methylammonium lead triiodide perovskite ($MAPbI_3$ = $CH_3NH_3PbI_3$). Formamidinium lead triiodide ($FAPbI_3$ = $CH(NH_2)_2PbI_3$) on the other hand has received far less attention, perhaps because the choice of the A cation in the ABX_3 perovskite structure was thought to have a relatively subtle influence on the electronic properties.[18−21] Here we investigate $FAPbI_3$ to highlight clear differences with $MAPbI_3$ in terms of optoelectronic and structural properties and their dependence on temperature.

The variation in dielectric environment resulting from differences in the choice of A cation has the potential to influence the Coulomb interactions in hybrid perovskites. As a consequence of such Coulomb interactions, discrete excitonic states may be formed from bound electron and hole pairs at energies below the band gap.[22,23] Stronger Coulomb interactions in a material lead to a larger exciton binding energy and also enhance the optical absorption coefficient of the above-gap unbound continuum states for charge carriers.[22,23] The value of the exciton binding energy E_X in $MAPbI_3$ has been repeatedly investigated by numerous methods, including absorption onset modeling, photoluminescence (PL) quenching, and magnetoabsorption, as summarized in ref 10. However, reported values vary widely[10] owing to the challenges of directly observing excitonic transitions in these materials. Accurate knowledge of E_X for a range of hybrid perovskites would be highly useful for the development of perovskite solar cells, given that excitons can only contribute to a photocurrent if efficient exciton dissociation is able to occur at the operating temperature of the device.[24,25]

Intraexcitonic transitions take place upon absorption of low-energy photons, typically on the order of a few millielectron volts. Direct observation of such transitions can therefore be made with light in the terahertz frequency regime (1 THz = 4.1 meV) at low temperature, for which excitonic states persist against thermally induced dissociation. In the absence of an electron−hole population in the conduction and valence bands of the hybrid perovskite, terahertz absorption may also result

Received: May 25, 2018
Accepted: July 23, 2018
Published: July 23, 2018

DOI: 10.1021/acs.jpclett.8b01628
J. Phys. Chem. Lett. 2018, 9, 4502−4511

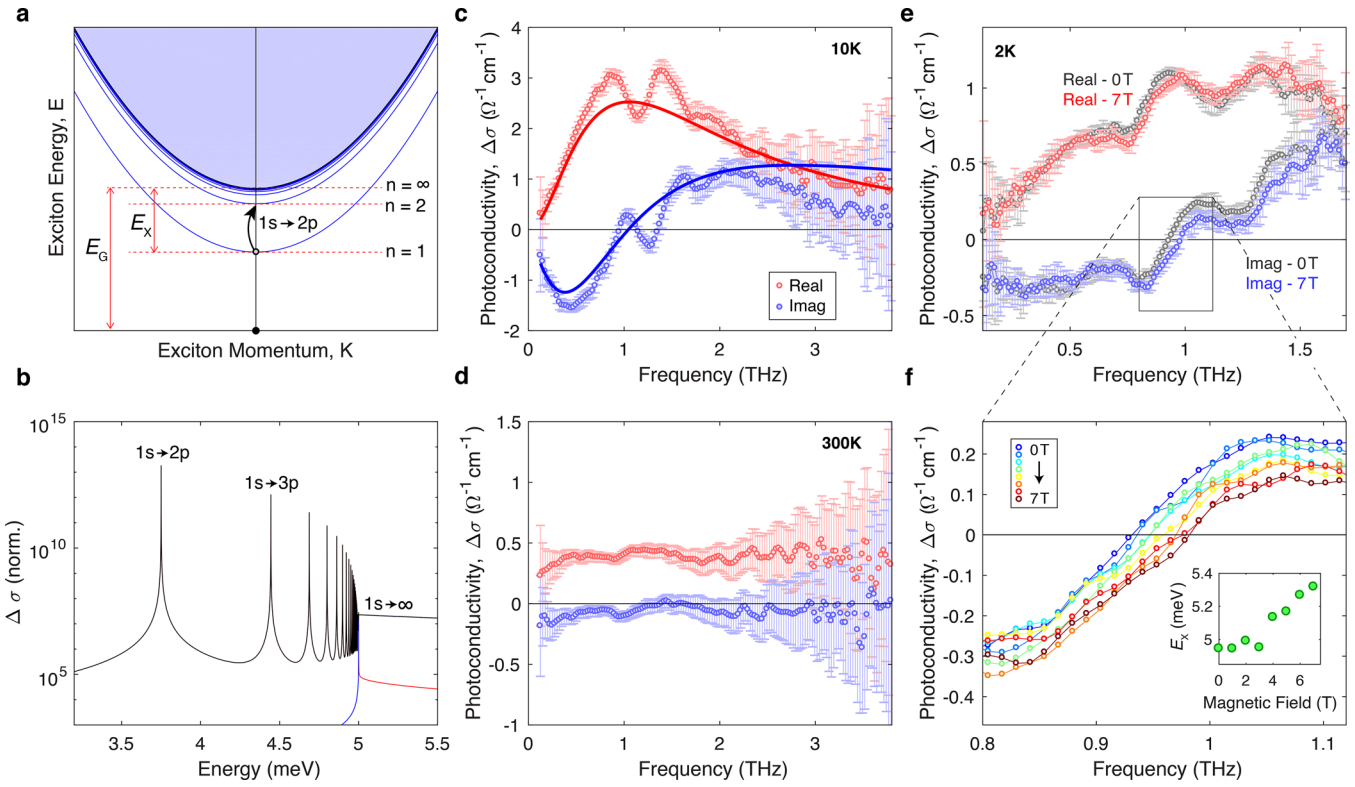

Figure 1. Intraexcitonic transitions in $FAPbI_3$ measured by photoconductivity spectra. (a) Exciton dispersion relation showing the discrete energy levels of the exciton at energies below the band gap. (b) Modeled photoconductivity spectra shown on a logarithmic scale, calculated from an intraexcitonic model of a three-dimensional material with minimal broadening ($\Gamma = 1$ μeV; see the Supporting Information for details). The bound states are shown as a red line, and the continuum states are shown as a blue line, with the total shown superimposed in black. (c,d) Photoconductivity spectra of $FAPbI_3$ at 10 and 300 K, respectively. Oscillations in the spectra at 10 K between 0.8 and 1.7 THz are attributed to modulation of the photoconductivity by phonon modes. Increasing error bars at higher frequencies demonstrate the bandwidth of the measurement. (e) Photoconductivity spectra at a magnetic fields of 0 T (gray) and 7 T shown as red and blue for the real and imaginary parts, respectively. The spectrum at 7 T is found to be blue-shifted with respect to the spectrum at 0 T. (f) Imaginary part of the photoconductivity spectra, taken at magnetic fields between 0 T (blue) and 7 T (red) in steps of 1 T. The inset in (f) shows the extracted exciton binding energy as a function of magnetic field. Photoconductivity spectra were measured by OPTPS using a 400 nm pump with a fluence of ~10 μJ cm^{-2} and a probe delay of 30 ps (c,d) and 500 ps (e,f).

from excitation of lead halide lattice vibrations.[26−28] Crucially, the presence of an additional optical pulse in optical pump terahertz probe spectroscopy (OPTPS) will photoexcite electrons and holes, allowing a distinction to be made between such vibrational signatures and transitions between excitonic states. OPTPS has therefore been successfully used for determination of the exciton binding energy in classical inorganic semiconductors such as GaAs−AlGaAs quantum wells.[29−32] Here, photoexcitation of the semiconductor initially generates a highly nonequilibrium distribution of electrons and holes in the conduction and valence bands, respectively, whose thermalization occurs on a subpicosecond time scale, populating exciton states.[33] In OPTPS, a subsequently arriving broad-band terahertz pulse (0−15 meV) then probes the presence of excitons through intraexcitonic transitions that predominantly occur between the 1s and *n*p states, from whose energy the exciton binding energy can be directly inferred.

Aside from a focus on excitonic effects, the mechanisms determining the charge-carrier mobility in hybrid perovskites have also recently received much scrutiny.[2,20,34] An understanding of the interactions and scattering processes that limit the mobility of charge carriers is highly useful because it can aid in the design of novel hybrid perovskites optimized for photovoltaic applications.[2,34,35] It had recently been shown that the charge-carrier mobility in hybrid lead halide perovskites is mostly governed by Fröhlich[36] interactions between longitudinal optical phonons and charge carriers.[20] However, such assertions could potentially be at odds with the $T^{-1.5}$ temperature dependence of the charge-carrier mobility μ repeatedly observed[5,37−39] for $MAPbI_3$. Recent theoretical calculations[34] have suggested that in the limit of Fröhlich coupling the temperature dependence should instead be closer to $\mu \approx T^{-0.5}$. For $FAPbI_3$, on the other hand, knowledge of the dependence of the charge-carrier mobility on temperature is still outstanding. Here, OPTPS offers a noncontact method to probe the charge-carrier mobility that allows exploration of such intrinsic effects because the high-frequency AC conductivity spectrum probes the charge-carrier motion on small length scales that are less affected by extrinsic limitations, such as those posed by grain boundaries.

In this study, we utilize OPTPS to explore the photoconductivity and magnetophotoconductivity of $FAPbI_3$. At low temperature (10 K), we observe direct transitions between the 1s and *n*p excitonic levels, from which we determine a remarkably small exciton binding energy of 5.3 meV. Magneto-OPTPS further reveals that the value of the exciton binding energy increases with magnetic field. Terahertz time domain spectroscopy (TDS) of $FAPbI_3$ is used to investigate changes in the phonon modes of Pb−I bond vibrations as a function of temperature. The phonon modes of $FAPbI_3$ show no splitting

DOI: 10.1021/acs.jpclett.8b01628
J. Phys. Chem. Lett. 2018, 9, 4502−4511

in the lower-temperature phase, which is in direct contrast with behavior observed for $MAPbI_3$, highlighting differences in crystal structure. We further examine the temperature dependence of the exciton binding energy and band gap energy for $FAPbI_3$ through modeling of the absorption coefficient near the band edge. We observe smooth changes in values with temperature, which contrasts greatly with the discontinuities in the band gap and exciton binding energy typically observed at the orthorhombic-to-tetragonal phase transition in $MAPbI_3$. In addition, we find that the charge-carrier mobility in $FAPbI_3$ exhibits a temperature dependence of $T^{-0.5}$, again in contrast with previous observations for $MAPbI_3$ but in excellent agreement with theoretical expectations for electron−phonon coupling dominated by Fröhlich interactions.

We commenced our study by investigating intraexcitonic transitions between discrete excitonic levels in order to obtain an accurate value of the exciton binding energy in $FAPbI_3$. Such discrete energy levels are described by the expression $E_n = E_G - E_X/n^2$, where E_G is the energy of the band gap, E_X is the exciton binding energy, and n is a positive integer. Figure 1a illustrates schematically how such excitonic effects modify the dispersion diagram, leading to an exciton−momentum dispersion relation in the two-particle picture as a function of the center-of-mass momentum, K, of the exciton. Because we use THz photoconductivity spectroscopy in this study to explore the interexcitonic resonances, Figure 1b illustrates the expected photoconductivity spectrum of intraexcitonic transitions, calculated for a material with minimal broadening (Γ = 1 μeV; see the Supporting Information for details). We note that the photoconductivity, $\Delta\sigma$, is related to the change in dielectric function, $\Delta\epsilon$, upon photoexcitation by $\Delta\sigma = -i\epsilon_0\omega\Delta\epsilon$. Therefore, the measurement of $\Delta\sigma$ for the exciton is equivalent to the polarization response caused by the interexcitonic transitions. Figure 1b reveals sharp lines associated with intraexcitonic transitions (1s → np), with the lowest-energy peak being associated with the 1s to 2p transition. The oscillator strength of transitions between the 1s and np levels decreases rapidly for increasing n, which results in weaker absorption into higher levels from the ground state (see the Supporting Information).[40] As n tends to infinity, the photoconductivity transforms into a pseudocontinuum, and for transition energies above the binding energy, the exciton dissociates into unbound continuum states.

To explore such effects experimentally, we measured the THz photoconductivity spectra of $FAPbI_3$ at 10 K, where stable excitons are able to persist. Figure 1c shows these data together with a fit for the exciton resonance, given by a sum of Lorentz oscillators with resonant energies $E_{1s-np} = E_X[1 - (1/n^2)]$ for transitions between the 1s and np states and assuming a magnitude proportional to the oscillator strength (see the Supporting Information for full details). Our use of a recently developed terahertz emitter based on the inverse spin Hall effect[41−43] here allows for a large spectral bandwidth and therefore clear observation of a resonance near 1 THz, given by the peak in the real part, and a matching zero-crossing in the imaginary part of the photoconductivity. This photoconductivity spectrum of the excitonic resonance in $FAPbI_3$ is broadened most likely by a combination of lifetime effects, defects in the crystal, and interactions with phonons, such that individual transition lines cannot be resolved. From the full fit based on the modeled 1s−np transitions, we extract an exciton binding energy of 5.3 meV for $FAPbI_3$ at 10 K. This value is toward the lower end of the range of values that have been reported for the related $MAPbI_3$,[10] but it is not atypical for a semiconductor of this band gap energy.[44] The additional modulations in the spectrum at approximately 1 and 1.6 THz are attributed to phonon modes that couple to the photoexcited species, as observed previously for $MAPbI_3$[26] and in agreement with the strong electron−phonon coupling reported for these materials.[20]

An unambiguous assignment of the observed resonance to excitons requires us to rule out alternative origins. In principle, there is a reasonable possibility that bulk plasmons could produce resonance in the photoconductivity spectra when these collective free-charge oscillations interact with the boundaries of their containing medium. The resonant frequency of plasmons is proportional to the square root of the charge-carrier density;[45] therefore, we measured the photoconductivity spectra for different excitation fluences corresponding to different initially generated charge-carrier densities (see Figure S4 in the Supporting Information). We were unable to discern any significant shift in the resonant frequency as a function of fluence, which verifies that the observed photoconductivity does not originate from a plasmon resonance.

We further find that as we raise the temperature to 300 K, the photoconductivity no longer exhibits a resonance within the observation window (Figure 1d). The disappearance of the resonance is further proof of an excitonic effect because excitons are expected to dissociate at thermal energies (300 K ≡ 26 meV) significantly higher than the exciton binding energy. In contrast, a bulk plasmon response would be expected to persist to higher temperatures. We find that, instead, the photoconductivity at 300 K (Figure 1d) reflects the Drude response of charge carriers, as observed previously for metal halide perovskites at room temperature.[8,26] The Drude model of conductivity applies the principles of kinetic theory to the charge carriers in a material.[46,47] In contrast with the photoconductivity spectra of excitons, a Drude response is characterized by (i) a nonzero real component and a zero imaginary component at zero frequency and (ii) a positive imaginary component maximum at an angular frequency equal to the scattering rate. Therefore, the observed zero imaginary part and constant positive real part across the photoconductivity spectrum derive from a free charge-carrier conductivity response with a scattering rate that lies beyond our measurement bandwidth.

The value of 5.3 meV that we determine for the low-temperature phase of $FAPbI_3$ is smaller than that proposed previously from temperature-activated PL intensity measurements (18 meV).[48] However, the temperature dependence of the PL intensity is also influenced by variations in trap-mediated charge-carrier recombination[37,49] and in bimolecular charge-carrier recombination,[23] which results in a complex temperature dependence that is difficult to decouple from effects attributable solely to exciton dissociation. In addition, the value that we determine is somewhat lower than that derived from magnetoabsorption measurements.[50] However, because such techniques rely on an accurate extrapolation of binding energies to zero magnetic field,[50−52] we also explore here how the low-temperature photoconductivity resonance changes with magnetic field. Numerical variational calculations on hydrogenic systems in arbitrary magnetic fields performed by Aldrich and Greene[52] predict a rise in the exciton binding energy with increasing B-field, which has indeed been observed

DOI: 10.1021/acs.jpclett.8b01628
J. Phys. Chem. Lett. 2018, 9, 4502−4511

Table 1. Reported Crystal Phases of $FAPbI_3$ and $MAPbI_3$[a]

	α phase		β phase		γ phase	ref
$FAPbI_3$	$P3m1$ trigonal	←150 K→	$P3$ trigonal	←100 K→		53
	$Pm\bar{3}m$ cubic					54
	$Pm\bar{3}m$ cubic	←285 K→	$P4/mbm$ tetragonal	←140 K→	$P4/mbm$ tetragonal	55
	$Pm\bar{3}m$ cubic	←290−350 K† →	$P6_3/mmc$ hexagonal	←100−175 K→	$P6_3/m$ hexagonal	56
	$Pm\bar{3}m$ cubic	←280 K→	$P4/mbm$ tetragonal	←140 K→	$P4bm$ tetragonal	57
$MAPbI_3$	$Pm\bar{3}m$ cubic	←327.4 K→	$I4/mcm$ tetragonal	←162.2 K→	$Pnma$ orthorhombic	58

[a]While a consensus of the crystal phases of $MAPbI_3$ has been reached, a unified picture of the crystal phases of $FAPbI_3$ is still outstanding. Note† that Chen et al.[56] reported different phase transition temperatures for heating and cooling.

in inorganic semiconductors such as GaAs.[32] Accurate modeling of the magnetoabsorption of the exciton is therefore required for deduction of the exciton binding energy from this method,[50−52] with differences between the theoretical and actual dependence of the exciton binding energy on magnetic field resulting in errors in the estimation of the zero-field exciton binding energy. As a direct measure of how the exciton binding energy of $FAPbI_3$ changes in a moderate magnetic field between 0 and 7 T, we exploit OPTPS to observe the excitonic resonance energy as a function of magnetic field. Figure 1e shows the photoconductivity spectra of $FAPbI_3$ in the presence of a magnetic field of 0 T shown in gray and 7 T shown in red for the real and blue for the imaginary parts. The spectrum at 7 T is blue-shifted with respect to the spectrum at 0 T. Zooming in on the imaginary component at the zero conductivity crossover point near 1 THz, Figure 1f demonstrates clearly the increasing resonant frequency as the magnetic field is increased in 1 T steps from 0 to 7 T. The inset shows the increase in exciton binding energy deduced from fits based on the modeled 1s−*n*p transitions to the data. While we do find an increase in exciton binding energy with magnetic field, the magnitude of the increase is of a significantly smaller extent than calculations would predict.[51,52] We therefore suggest that the discrepancy between the theoretically expected and the experimentally observed dependence of the exciton binding energy on the magnetic field is the reason for the elevated exciton binding energy suggested for $FAPbI_3$ from magneto-absorption experiments.

One way by which hybrid perovskites differ from classical inorganic semiconductors is by exhibiting a plethora of structural phase transitions at different temperatures. However, while the structural phases of $MAPbI_3$ and their transition temperatures are well-established, the picture for $FAPbI_3$ is far less clear.[53−58] An important starting point for structural calculations is accurate knowledge of the energy of phonon modes of a material's lattice structure. We therefore use absorption spectra at terahertz frequencies to investigate the phonon modes in $FAPbI_3$ as a function of temperature and contrast our findings with what is observed in $MAPbI_3$.

To illustrate the inconsistencies in the literature on the phase transitions among the α, β, and γ (high- to low-temperature) phases of $FAPbI_3$, we present in Table 1 details of previously reported structures. The structural phases of $MAPbI_3$ and the transition temperatures are well-established, and there is generally good agreement with the parameters shown in the last line of Table 1. However, the table highlights a large spread in reported structures for $FAPbI_3$, with some sort of consensus only existing for the cubic high-temperature α phase. In addition to the determination of structural phases for bulk $FAPbI_3$, other studies have reported the structural phases of nanocrystals, with the nanocrystal form of $FAPbI_3$ taking a cubic form at room temperature.[59] For $FAPbI_3$, the phase transitions between both the α−β and β−γ phases appear to occur over a large temperature region (>50 K), which has been attributed to the nontrivial reorganization of atoms owing to the lack of a group−subgroup relation between space groups of the phases and also the different temperature-dependent rotational dynamics of the FA cation, compared to the MA cation.[55,56,60] Upon the transition from the high-temperature, high-symmetry α phase to the β phase, the symmetry is lowered by the introduction of Pb−I octahedra tilting. The transition from the β phase to the low-temperature γ phase is accompanied by freezing of the cations in random orientations.[53] Interchanging the cation between MA and FA therefore has a significant impact on the structural properties of the material. As we show below, such changes may also affect the optical properties, as evident from differences in the phonon modes and optical absorption.

The dark terahertz transmission, T, of a $FAPbI_3$ thin film was measured by TDS (see the Experimental Details). Absorption, α_{Abs}, was calculated from the measured transmission using the expression $\alpha_{Abs} \propto -\ln(|T|)$. Figure 2a reveals two phonon modes at approximately 0.85 and 1.65 THz for $FAPbI_3$, which we attribute to vibrations of the Pb−I bonds, in analogy with $MAPbI_3$.[26−28] We find that in $FAPbI_3$ these modes are largely unchanged over the temperature range from 10 to 300 K, despite the up to two phase transitions occurring over that range, i.e., from the low-temperature γ phase to the β phase between 100 and 175 K and potentially on to the α phase near 290 K.[55,56] There is only a small shift in the lowest-frequency mode, from 0.8 THz at low temperature to 0.9 THz at room temperature. In contrast, Figure 2b shows the absorption of phonon modes in $MAPbI_3$, which change significantly between 10 and 300 K, that is, the two high-temperature phonon modes observed in the β phase split into four phonon modes in the γ phase.[27,28] Such differing behavior can be attributed to the link between the dynamics of the Pb−I octahedra and the orientation of the organic cation.[61] In the two high-temperature phases of $MAPbI_3$ (α and β), both tumbling (rapid reorientation of the C−N axis) and twisting (rotation

DOI: 10.1021/acs.jpclett.8b01628
J. Phys. Chem. Lett. 2018, 9, 4502−4511

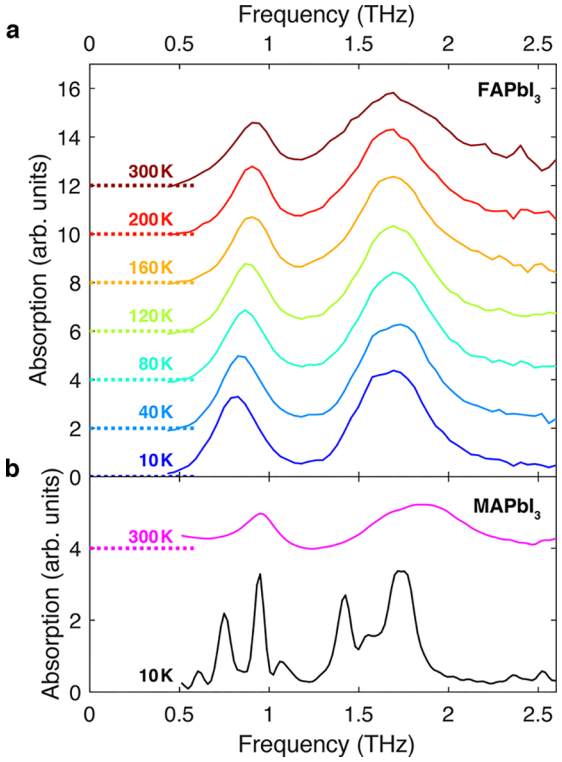

Figure 2. Lead iodide phonon absorption spectra. (a) Absorption spectra of $FAPbI_3$ at terahertz frequencies for different temperatures. The two peaks at approximately 0.8−0.9 and 1.65 THz are attributed to Pb−I vibrations. The dashed lines show the offsets by which each spectrum has been shifted for clarity. (b) Absorption spectra of $MAPbI_3$ at 10 and 300 K at terahertz frequencies. In contrast to $FAPbI_3$, the lead halide phonon modes of $MAPbI_3$ split into four modes at low temperature.[27,28] The absorption, α_{Abs}, was calculated from the measured transmission, T, using the expression $\alpha_{Abs} \propto -\ln(|T|)$.

about the C−N axis) of the MA cation are possible; however, only twisting is possible in the γ phase.[62,63] The low-temperature rotational dynamics of the FA cation have been explored to a much lesser extent. Carignano et al. have performed molecular dynamic simulations of $FAPbI_3$ and found that at high temperatures (450 K) FA rotations about the N−N axis and orthogonal to the N−N axis are possible. Upon lowering the temperature from 450 to 300 K, the FA cation mobility reduces and rotations are nearly all about the N−N axis.[61] While at lower temperatures the rotational freedom of MA in $MAPbI_3$ is significantly reduced, the FA cation in $FAPbI_3$ appears to be less affected.[64] In addition, FA cations have a larger effective ionic radius than MA cations, which results in $FAPbI_3$ having a larger unit cell than $MAPbI_3$.[54] In general, we conclude that the differences between $FAPbI_3$ and $MAPbI_3$ in terms of the temperature-dependent phonon mode spectra is most likely derived from the different dynamics of the FA and MA cations in the lead iodide cage.

The magnitude of the dipole moments carried by the chosen A cation could potentially influence the polarizability of the perovskite.[65] Any changes in the dielectric function will have an effect on charge-carrier screening and therefore the exciton binding energy. To observe the effect of structural changes with temperature on the exciton binding and band gap energy, we measured the reflection (R) and transmission (T) spectra of $FAPbI_3$ between 4 and 300 K using a Fourier transform infrared (FTIR) spectrometer with the sample mounted in a gas-exchange cryostat (see the Experimental Details section). Reflection−transmission spectra were converted to absorption coefficient spectra ($\alpha(E)$) using $\alpha = -(1/d)\ln(T/(1-R))$, where d is the thickness of the $FAPbI_3$ film.

Figure 3a presents the resulting absorption coefficient spectra of $FAPbI_3$ as a two-dimensional color map versus temperature and energy. Outside of the phase transition region between ∼100 and 160 K, the absorption onset generally blue shifts with increasing temperature in both the high- and low-temperature phases. This general trend in band gap energy with temperature is similar to what has been observed for $MAPbI_3$[20,37] but is in contrast with the typical behavior for III−V inorganic semiconductors, such as GaAs.[66]

To extract values for the band gap energy and exciton binding energy, the absorption spectrum has to be modeled to include both electronic transitions between electron−hole continuum and bound excitonic states, as illustrated in Figure 1a. Elliott developed a theory on the intensity of optical absorption by excitons,[22] which has previously been applied to model the absorption onset for $MAPbI_3$.[23,67,68] Here we apply this theory for $FAPbI_3$ to determine the band gap (Figure 3c) and the exciton binding energy (Figure 3d) as a function of temperature (see the Supporting Information for a full description of the fitting function used). An example fit of Elliott's expression to the absorption onset at one temperature (4 K) is shown in Figure 3b. We note that, unlike for $MAPbI_3$, which at low temperature has been found to exhibit a sharp peak below the gap as a result of absorption into bound excitonic states,[23,67] $FAPbI_3$ only exhibits a much weaker enhancement. Our fits of Elliott's expression to the absorption onset show that the lack of a pronounced excitonic peak for $FAPbI_3$ at 4 K is not the result of increased broadening but is rather derived from a low value of the exciton binding energy, in agreement with the low-energy excitonic resonance that we observed in our OPTP measurements discussed above.

From the dependence of the band gap energy on temperature (Figure 3c), we can clearly discern a region between 100 and 160 K (shaded gray) over which a change from the γ phase to the β phase occurs. This transition temperature range agrees well with that deduced from previous XRD measurements.[55,56] We note that the change in band gap energy at the phase transition that we observe here for $FAPbI_3$ is markedly different from that previously reported for $MAPbI_3$,[23,37] which typically displays a sharp discontinuity in band gap on the order of 100 meV. In contrast, the change in band gap energy between the β and γ phases in $FAPbI_3$ is remarkably smooth, occurring over a wide temperature range (∼60 K) and only leading to a downshift of ∼20 meV with increasing temperature. This contrasting behavior in terms of band gap changes at the phase transition of $FAPbI_3$ and $MAPbI_3$ is likely to arise from the difference in molecular dynamics of the organic cations already mentioned above. It has been suggested that for $MAPbI_3$ reorientation of the dipole (tumbling of C−N axis) completely freezes out once the low-temperature γ phase is entered. However, some degree of dipole reorientation (about the N−N axis) is preserved in $FAPbI_3$ in both the β and γ phases near the transition temperature,[60] which will lead to the much more gradual change in optical properties that we report here.

The other parameter obtained from fits of Elliott's theory to the band edge is the exciton binding energy, shown in Figure

DOI: 10.1021/acs.jpclett.8b01628
J. Phys. Chem. Lett. 2018, 9, 4502−4511

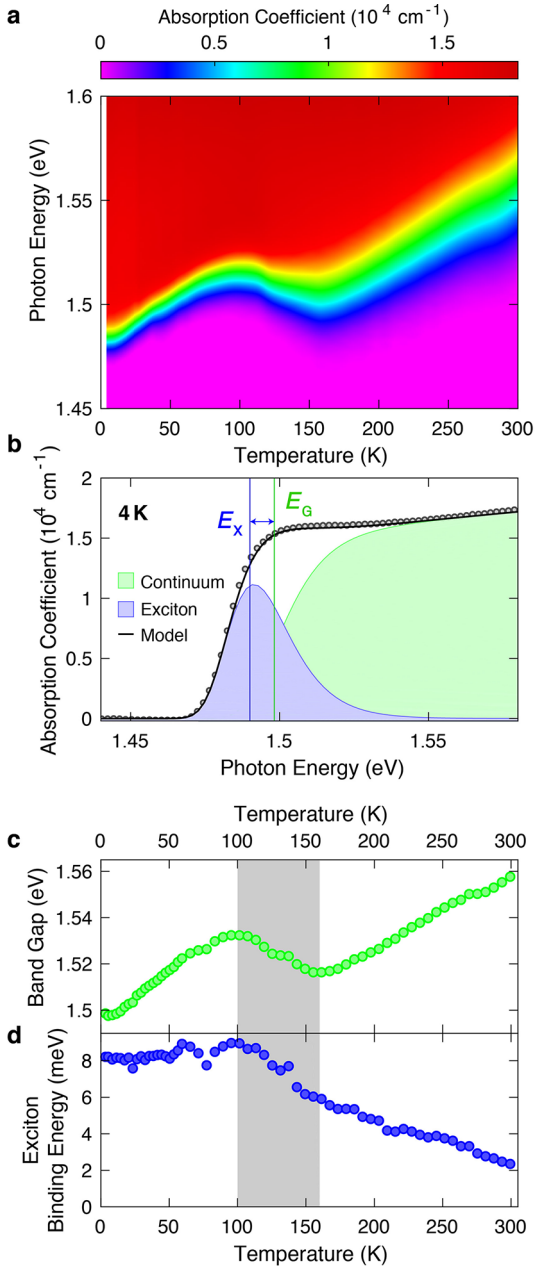

Figure 3. Absorption coefficient of $FAPbI_3$ at optical frequencies. (a) Temperature-dependent absorption spectra of $FAPbI_3$ displayed as a two-dimensional color map. (b) Absorption spectrum at 4 K, measured by FTIR spectroscopy. Experimental data are shown as gray circles, and a fit based on Elliott's theory is shown as a solid black line. Contributions to the absorption coefficient from bound excitonic and continuum states are displayed by shaded blue and green areas, respectively. The vertical green line shows the band gap energy, E_G, and the difference between blue and green vertical lines is the exciton binding energy, E_X. (c,d) Band gap and exciton binding energy extracted from such fits to the absorption spectra. The gray area displays the region of the observed β–γ phase transition of $FAPbI_3$ between 100 and 160 K.

3d as a function of temperature. In the low-temperature γ phase, the exciton binding energy is approximately constant with a value near 8 meV. Over the phase transition from the γ to β phase (beginning at 100 K through to 160 K), a steady decline in the exciton binding energy occurs. The exciton binding energy continues to decrease with increasing temperature throughout the β phase, reaching a value of 2.4 meV at room temperature. We recently extracted the exciton binding energy for $MAPbI_3$[23] through an identical method of Elliott fitting of the absorption onset and note two main differences with the data reported here for $FAPbI_3$. The first is that the overall value of the binding energy for $FAPbI_3$ is generally lower by a factor of 2–3 than that for $MAPbI_3$ across the temperature range. The second is that, while both $FAPbI_3$ and $MAPbI_3$ exhibit a near-constant value of the exciton binding energy in the γ phase, the behavior around the phase transition is markedly different. For $MAPbI_3$, a sharp decrease in binding energy by approximately 5 meV has been found to occur over a very narrow temperature range.[23] However, here we observe that there is no sudden discontinuity in the exciton binding energy for $FAPbI_3$ (Figure 3d) but rather a gradual decrease over a broad temperature range. The absence of discontinuities in the band gap and exciton in $FAPbI_3$ and the presence of discontinuities in $MAPbI_3$ suggest a different nature of the phase transition and is attributed to differences in the dynamics and structural influence of the FA and MA cations on $FAPbI_3$ and $MAPbI_3$, respectively. We note that these observations for the exciton binding energy are in agreement with temperature-dependent measurements of the dielectric permittivity of $FAPbI_3$, which was found to change smoothly across the phase transition.[55] The inherent dependence of the exciton binding energy on the inverse of the square of the dielectric permittivity[10] is therefore reflected in the differences in the nature of the phase transition and the associated changes in polarizability of the material.

We note that the value that we extract for the exciton binding energy at low temperature is slightly higher for the Elliott approach compared with that determined from terahertz spectroscopy (OPTP). We suggest that these slight discrepancies may arise from the difficulties in obtaining a satisfactory fit of Elliott's theory to the absorption onset over a sufficiently wide energy range.[23,68] As we have shown recently, Elliott's theory does not account for the possible presence of multiple electronic transitions, nonparabolic bands, and an energy dependence of the associated matrix elements.[23] As a result, the shape of the free (uncorrelated) continuum-state absorption may deviate from the square-root dependence on energy above the gap. As we discuss in more detail in the Supporting Information, for $FAPbI_3$, these deviations seem to cause a slight upshift in the value of the exciton binding energy extracted from the Elliott approach.

Another electronic parameter that underpins the operation of solar cells is the charge-carrier mobility. For charge carriers to be extracted in a photovoltaic device, charge mobilities need to be sufficiently high such that within the carrier lifetime the charges are able to reach the electron and hole transport layers.[11] Terahertz photoconductivity measurements are an excellent choice for studying the charge-carrier mobility of a material as the method does not rely on electrical contacts that would otherwise complicate the measurement.

The mechanisms limiting the mobility of charge carriers in metal halide perovskites are a subject of much current debate. While some hybrid perovskites can still show dependences on extrinsic factors, such as electron scattering off grain boundaries and defects, it has recently been argued that high-performing materials such as $MAPbI_3$ and $FAPbI_3$ are nearing the limit of what is intrinsically achievable.[2] Analysis of the temperature-dependent emission-line broadening in $MAPbI_3$ and $FAPbI_3$[20] further revealed that Fröhlich

DOI: 10.1021/acs.jpclett.8b01628
J. Phys. Chem. Lett. 2018, 9, 4502–4511

interactions between charge carriers and longitudinal optical (LO) phonons are the dominant intrinsic mechanism limiting charge-carrier motion. Such a mechanism qualitatively agrees with the strong increase observed in the charge-carrier mobility of $MAPbI_3$ as the temperature is lowered.[5,37−39] However, such measurements have consistently yielded[5,37−39] a dependence of the charge-carrier mobility μ on temperature T according to $\mu \propto T^w$, with $w = -1.5$. This experimentally determined value of the exponent w for $MAPbI_3$ does not agree with the value of ∼−0.5 proposed recently[34] as a suitable high-temperature approximation to the charge-carrier mobility expected according to Hellwarth and Biaggio[69] when Fröhlich interactions dominate.

To assess whether such discrepancies also manifest themselves in $FAPbI_3$, we used OPTP to measure the effective charge-carrier mobility as a function of temperature for $FAPbI_3$ (see the Experimental Details section and Supporting Information for experimental details). Figure 4 shows the resulting data together with a best fit to $\mu \propto T^w$ over the temperature range of 60−300 K, which yields a value of $w = -0.53$, very close to what would theoretically be expected for $MAPbI_3$ when subject to Fröhlich interactions.[34] We note that this fit excluded data points below 60 K as excitonic effects may become more dominant here ($k_b \times 60\ K \leq 5.3$ meV), and hence, measurements of the effective charge-carrier mobility no longer fully reflect the values of the charge-carrier mobility in the material (see the Supporting Information). To indicate this, the dashed line is extrapolated from the fit, at temperatures below 60 K.

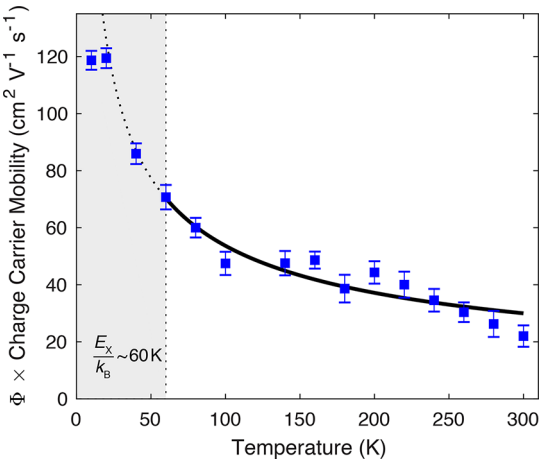

Figure 4. Effective charge-carrier mobility $\phi\mu$ as a function of temperature for a thin film of $FAPbI_3$. Here, μ is the charge-carrier mobility and ϕ the photon-to-free-charge branching ratio, which is expected to decrease from a high-temperature value of 1 when the temperature is lowered below the value of $E_X/k_b \approx 60$ K and excitons become thermally stable. The solid line shows a fit of $\mu \propto T^w$ to the data for temperatures 60 K and above. A power-law behavior with an exponent of $w = -0.53$ is found, in agreement with predictions[34] based on charge-carrier interactions with polar optical phonons.[20]

Our results thus reveal that the discrepancy between the theoretically expected and experimentally determined temperature dependence of the charge-carrier mobility for $MAPbI_3$ is not a universal feature of lead iodide perovskites. For $FAPbI_3$, excellent agreement with the dependence expected for halide perovskites is obtained, suggesting that a Fröhlich picture of charge-carrier interactions with phonons is fully appropriate. While we cannot conclusively determine here the reasons for the discrepancy between theory and experiments observed in $MAPbI_3$, we propose that they may lie in issues with phase retention observed in $MAPbI_3$. Experiments have repeatedly shown that thin films of $MAPbI_3$ may have remnant domains that contain regions of different crystallographic structure.[70] For example, additional PL features in the low-temperature orthorhombic phase below 160 K have been attributed to the presence of remnant tetragonal domains over a relatively large temperature range.[70] Such regions could represent barriers to charge-carrier motion, whose prevalence depends on the material temperature, leading to a deviation from the intrinsic behavior expected from Fröhlich interactions alone. For $FAPbI_3$, on the other hand, such minority-phase inclusions have been shown to be absent,[20] and hence, the expected[34,69] temperature dependence of $\mu \propto T^{-0.5}$ is indeed observed.

In conclusion, our temperature-dependent studies of $FAPbI_3$ have revealed significant differences in the optoelectronic properties in comparison with $MAPbI_3$. We directly observed intraexcitonic transitions in $FAPbI_3$ from which we determined the exciton binding energy to be 5.3 meV at 10 K, which is comparable to the low end of the spectrum of reported values for $MAPbI_3$. We further examined how parameters critical to the operation of photovoltaic cells, such as the exciton binding energy, band gap, vibrational properties, and charge-carrier mobilities, vary with temperature and across phase transitions. We found that, in contrast to $MAPbI_3$, the band gap and exciton binding energy vary smoothly over a range of 100−160 K at the β to γ phase transition in $FAPbI_3$. Such absence of clear discontinuities for $FAPbI_3$ most likely results from the rotational freedom of the FA dipole moment being reduced only gradually upon entry into the γ phase, whereas in $MAPbI_3$, MA dipole rotation is frozen out abruptly over a narrow temperature range. We also demonstrated that such structural changes manifest themselves in the IR phonon signatures associated with the lead halide sublattice vibrations. The two phonon modes observed in the β phase are largely unchanged for $FAPbI_3$ upon entry into the γ phase, while for $MAPbI_3$, a splitting into four phonon modes is observed. Finally, we revealed that the charge-carrier mobility in $FAPbI_3$ exhibits a clear $T^{-0.5}$ trend with temperature, in excellent agreement with theoretical predictions for halide perovskites whose electron−phonon interactions are governed by the Fröhlich mechanism, but in contrast to the $T^{-1.5}$ dependence previously observed for $MAPbI_3$. The contrasting temperature-dependent behavior of excitons, phonons, electronic transitions, and charge-carrier mobilities in $MAPbI_3$ and $FAPbI_3$ highlights the impact of cation substitution not only on the structure of the perovskite but also on its optoelectronic properties.

EXPERIMENTAL DETAILS

$FAPbI_3$ Thin Film Fabrication by Vapor Deposition. Formamidinium lead triiodide thin films were fabricated using thermal co-evaporation in a vacuum chamber. We used a dual-source evaporation system (Kurt J. Lesker), with PbI_2 and FAI as precursors. Formamidinium iodide powder was obtained from Dyesol, and PbI_2 beads were from Alfa Aesar. The PbI_2 and FAI precursors were heated in separate crucibles until each of the precursors evaporated. During evaporation, the pressure in the chamber stayed at approximately 10^{-6} mbar. For FAI, the evaporation temperature was 150 °C, and PbI_2 was evaporated at 300 °C. The quartz substrates were mounted above the

DOI: 10.1021/acs.jpclett.8b01628
J. Phys. Chem. Lett. 2018, 9, 4502−4511

sources so that the vapors condensed onto the substrates and a $FAPbI_3$ film formed. The deposited films were annealed on a hot plate at 170 °C for 1 min to ensure that they were in the desired perovskite phase of $FAPbI_3$. We previously confirmed and reported that this deposition method results in smooth, uniform $FAPbI_3$ thin films.[16] The samples used in this study are from the same batch growth as that reported by Borchert et al.,[16] whose study provides a detailed characterization of the material including X-ray diffraction measurements, performance in photovoltaic cells, atomic force microscopy images of the surface, scanning electron microscopy images, UV/vis and near-IR absorption spectra, and PL lifetimes.

Terahertz Time Domain Spectroscopy (TDS). TDS was used to measure the absorption of phonon modes in $FAPbI_3$ and $MAPbI_3$. With TDS, the output of an amplified laser system with 30 fs pulses at a repetition rate of 5 kHz with a central wavelength of 800 nm and an average power of 4 W is split into two beam paths: a probe beam and a gate beam. Terahertz pulses are generated by the inverse-spin Hall effect.[41−43] Terahertz pulses are detected by electro-optic sampling using a 0.2 mm thick GaP(110) crystal, a Wollaston prism, and a pair of balanced photodiodes. Temperature-dependent TDS measurements were performed using a coldfinger cryostat (Oxford Instruments). By measuring $FAPbI_3$ on a quartz substrate and taking reference measurement of a quartz substrate, we can obtain the terahertz transmission in the time domain.

Optical Pump Terahertz Probe Spectroscopy (OPTPS). OPTPS was used to measure the photoconductivity of $FAPbI_3$. OPTPS extends the TDS technique to allow measurement of a sample in the photoexcited state. A schematic of the OPTPS setup is provided in the Supporting Information. In OPTPS, the sample is photoexcited by an optical pump and after a short time delay is probed with a terahertz pulse. The generation and detection of the terahertz pulse is the same as that in the TDS method detailed above. Transformation from the change in transmission with photoexcitation to photoconductivity is detailed in the Supporting Information. Magnetophotoconductivity measurements were measured by magneto-OPTPS, which is the same as OPTPS but conducted in the presence of a magnetic field (Oxford Instruments Spectromagnet). For magneto-OPTPS, terahertz pulse were generated using optical rectification using a ZnTe crystal and were detected using a ZnTe (110) crystal. Further experimental details have been detailed previously.[32]

Fourier Transform Infrared (FTIR) Spectroscopy. FTIR spectroscopy was used to determine the absorption coefficient spectra of $FAPbI_3$. Temperature-dependent reflectance transmission measurements of $FAPbI_3$ were performed using a FTIR spectrometer (Bruker Vertex 80v) with the sample mounted in a gas-exchange cryostat (Oxford Instruments OptistatCF2). A tungsten halogen lamp was used as the illumination source, with a CaF_2 beamsplitter and a silicon detector.

■ ASSOCIATED CONTENT

Supporting Information

The Supporting Information is available free of charge on the ACS Publications website at DOI: 10.1021/acs.jpclett.8b01628.

Details of the optical pump terahertz probe spectroscopy setup, details of photoconductivity of intraexcitonic transitions, analysis of photoconductivity measured by OPTPS, determination method of charge-carrier mobility from OPTPS, and extraction of the exciton binding energy from fitting of the absorption edge (PDF)

■ AUTHOR INFORMATION

Corresponding Authors

*E-mail: michael.johnston@physics.ox.ac.uk (M.B.J.).
*E-mail: laura.herz@physics.ox.ac.uk (L.M.H.).

ORCID

Michael B. Johnston: 0000-0002-0301-8033
Laura M. Herz: 0000-0001-9621-334X

Notes

The authors declare no competing financial interest.

■ ACKNOWLEDGMENTS

The authors gratefully acknowledge support from the Enginneering and Physical Sciences Research Council (EPSRC) through Projects EP/P033229/1, EP/P006329/1, and EP/L024667/1). J.B. is supported through a studentship by the EPSRC Centre for Doctoral Training in New and Sustainable Photovoltaics (EP/L01551X/1).

■ REFERENCES

(1) Yang, W. S.; Noh, J. H.; Jeon, N. J.; Kim, Y. C.; Ryu, S.; Seo, J.; Seok, S. I. High-performance Photovoltaic Perovskite Layers Fabricated Through Intramolecular Exchange. *Science* **2015**, *348*, 1234−1237.

(2) Herz, L. M. Charge-carrier Mobilities in Metal Halide Perovskites: Fundamental Mechanisms and Limits. *ACS Energy Lett.* **2017**, *2*, 1539−1548.

(3) Shrestha, S.; Matt, G. J.; Osvet, A.; Niesner, D.; Hock, R.; Brabec, C. J. Assessing Temperature Dependence of Drift Mobility in Methylammonium Lead Iodide Perovskite Single Crystals. *J. Phys. Chem. C* **2018**, *122*, 5935−5939.

(4) Turren-Cruz, S.-H.; Saliba, M.; Mayer, M. T.; Juarez-Santiesteban, H.; Mathew, X.; Nienhaus, L.; Tress, W.; Erodici, M. P.; Sher, M.-J.; Bawendi, M. G.; et al. Enhanced Charge Carrier Mobility and Lifetime Suppress Hysteresis and Improve Efficiency in Planar Perovskite Solar Cells. *Energy Environ. Sci.* **2018**, *11*, 78−86.

(5) Oga, H.; Saeki, A.; Ogomi, Y.; Hayase, S.; Seki, S. Improved Understanding of the Electronic and Energetic Landscapes of Perovskite Solar Cells: High Local Charge Carrier Mobility, Reduced Recombination, and Extremely Shallow Traps. *J. Am. Chem. Soc.* **2014**, *136*, 13818−13825.

(6) Crothers, T. W.; Milot, R. L.; Patel, J. B.; Parrott, E. S.; Schlipf, J.; Muller-Buschbaum, P.; Johnston, M. B.; et al. Photon Reabsorption Masks Intrinsic Bimolecular Charge-Carrier Recombination in $CH_3NH_3PbI_3$ Perovskite. *Nano Lett.* **2017**, *17*, 5782−5789.

(7) Zhao, D.; Yu, Y.; Wang, C.; Liao, W.; Shrestha, N.; Grice, C. R.; Cimaroli, A. J.; Guan, L.; Ellingson, R. J.; Zhu, K.; et al. Low-Bandgap Mixed TinLead Iodide Perovskite Absorbers With Long Carrier Lifetimes for All-Perovskite Tandem Solar Cells. *Nat. Energy* **2017**, *2*, 17018.

(8) Wehrenfennig, C.; Eperon, G. E.; Johnston, M. B.; Snaith, H. J.; Herz, L. M. High Charge Carrier Mobilities and Lifetimes in Organolead Trihalide Perovskites. *Adv. Mater.* **2014**, *26*, 1584−1589.

(9) Rehman, W.; Milot, R. L.; Eperon, G. E.; Wehrenfennig, C.; Boland, J. L.; Snaith, H. J.; Johnston, M. B.; Herz, L. M. Charge-Carrier Dynamics and Mobilities in Formamidinium Lead Mixed-Halide Perovskites. *Adv. Mater.* **2015**, *27*, 7938−7944.

(10) Herz, L. M. Charge-Carrier Dynamics in Organic-Inorganic Metal Halide Perovskites. *Annu. Rev. Phys. Chem.* **2016**, *67*, 65−89.

DOI: 10.1021/acs.jpclett.8b01628
J. Phys. Chem. Lett. 2018, 9, 4502−4511

(11) Johnston, M. B.; Herz, L. M. Hybrid Perovskites for Photovoltaics: Charge-Carrier Recombination, Diffusion, and Radiative Efficiencies. *Acc. Chem. Res.* **2016**, *49*, 146−154.
(12) Burschka, J.; Pellet, N.; Moon, S.-J.; Humphry-Baker, R.; Gao, P.; Nazeeruddin, M. K.; Grätzel, M. Sequential Deposition as a Route to High-Performance Perovskite-Sensitized Solar Cells. *Nature* **2013**, *499*, 316.
(13) Eperon, G. E.; Stranks, S. D.; Menelaou, C.; Johnston, M. B.; Herz, L. M.; Snaith, H. J. Formamidinium Lead Trihalide: A Broadly Tunable Perovskite for Efficient Planar Heterojunction Solar Cells. *Energy Environ. Sci.* **2014**, *7*, 982−988.
(14) Liu, M.; Johnston, M. B.; Snaith, H. J. Efficient Planar Heterojunction Perovskite Solar Cells by Vapour Deposition. *Nature* **2013**, *501*, 395.
(15) Patel, J. B.; Wong-Leung, J.; Van Reenen, S.; Sakai, N.; Wang, J. T. W.; Parrott, E. S.; Liu, M.; Snaith, H. J.; Herz, L. M.; Johnston, M. B. Influence of Interface Morphology on Hysteresis in Vapor-Deposited Perovskite Solar Cells. *Adv. Electron. Mater.* **2017**, *3*, 1600470.
(16) Borchert, J.; Milot, R. L.; Patel, J. B.; Davies, C. L.; Wright, A. D.; Martínez Maestro, L.; Snaith, H. J.; Herz, L. M.; Johnston, M. B. Large-Area, Highly Uniform Evaporated Formamidinium Lead Triiodide Thin Films for Solar Cells. *ACS Energy Letters* **2017**, *2*, 2799−2804.
(17) Wei, Z.; Chen, H.; Yan, K.; Yang, S. Inkjet Printing and Instant Chemical Transformation of a $CH_3NH_3PbI_3$/Nanocarbon Electrode and Interface for Planar Perovskite Solar Cells. *Angew. Chem.* **2014**, *126*, 13455−13459.
(18) Amat, A.; Mosconi, E.; Ronca, E.; Quarti, C.; Umari, P.; Nazeeruddin, M. K.; Grätzel, M.; De Angelis, F. Cation-Induced Band-Gap Tuning in Organohalide Perovskites: Interplay of Spin-Orbit Coupling and Octahedra Tilting. *Nano Lett.* **2014**, *14*, 3608−3616.
(19) Rehman, W.; McMeekin, D. P.; Patel, J. B.; Milot, R. L.; Johnston, M. B.; Snaith, H. J.; Herz, L. M. Photovoltaic Mixed-Cation Lead Mixed-Halide Perovskites: Links Between Crystallinity, Photo-Stability and Electronic Properties. *Energy Environ. Sci.* **2017**, *10*, 361−369.
(20) Wright, A. D.; Verdi, C.; Milot, R. L.; Eperon, G. E.; Pérez-Osorio, M. A.; Snaith, H. J.; Giustino, F.; Johnston, M. B.; Herz, L. M. Electron-Phonon Coupling in Hybrid Lead Halide Perovskites. *Nat. Commun.* **2016**, *7*, 11755.
(21) Umari, P.; Mosconi, E.; De Angelis, F. Infrared Dielectric Screening Determines the Low Exciton Binding Energy of Metal-Halide Perovskites. *J. Phys. Chem. Lett.* **2018**, *9*, 620−627.
(22) Elliott, R. J. Intensity of Optical Absorption by Excitons. *Phys. Rev.* **1957**, *108*, 1384.
(23) Davies, C. L.; Filip, M. R.; Patel, J. B.; Crothers, T. W.; Verdi, C.; Wright, A. D.; Milot, R. L.; Giustino, F.; Johnston, M. B.; Herz, L. M. Bimolecular Recombination in Methylammonium Lead Triiodide Perovskite Is an Inverse Absorption Process. *Nat. Commun.* **2018**, *9*, 293.
(24) D'Innocenzo, V.; Grancini, G.; Alcocer, M. J. P.; Kandada, A. R. S.; Stranks, S. D.; Lee, M. M.; Lanzani, G.; Snaith, H. J.; Petrozza, A. Excitons Versus Free Charges in Organo-Lead Tri-Halide Perovskites. *Nat. Commun.* **2014**, *5*, 3586.
(25) Patel, J. B.; Lin, Q.; Zadvorna, O.; Davies, C. L.; Herz, L. M.; Johnston, M. B. Photocurrent Spectroscopy of Perovskite Solar Cells Over a Wide Temperature Range from 15 to 350 K. *J. Phys. Chem. Lett.* **2018**, *9*, 263−268.
(26) Wehrenfennig, C.; Liu, M.; Snaith, H. J.; Johnston, M. B.; Herz, L. M. Charge-Carrier Dynamics in Vapour-Deposited Films of the Organolead Halide Perovskite $CH_3NH_3PbI_{3-x}Cl_x$. *Energy Environ. Sci.* **2014**, *7*, 2269−2275.
(27) La-O-Vorakiat, C.; Xia, H.; Kadro, J.; Salim, T.; Zhao, D.; Ahmed, T.; Lam, Y. M.; Zhu, J.-X.; Marcus, R. A.; Michel-Beyerle, M.-E.; et al. Phonon Mode Transformation Across the OrthohombicTetragonal Phase Transition in a Lead Iodide Perovskite $CH_3NH_3PbI_3$: A Terahertz Time-Domain Spectroscopy Approach. *J. Phys. Chem. Lett.* **2016**, *7*, 1−6.
(28) Perez-Osorio, M. A.; Milot, R. L.; Filip, M. R.; Patel, J. B.; Herz, L. M.; Johnston, M. B.; Giustino, F. Vibrational Properties of the Organic-Inorganic Halide Perovskite $CH_3NH_3PbI_3$ from Theory and Experiment: Factor Group Analysis, First-Principles Calculations, and Low-Temperature Infrared Spectra. *J. Phys. Chem. C* **2015**, *119*, 25703.
(29) Huber, R.; Schmid, B. A.; Kaindl, R. A.; Chemla, D. S. Femtosecond THz Studies of Intra-Excitonic Transitions. *Phys. Status Solidi B* **2008**, *245*, 1041−1048.
(30) Huber, R.; Kaindl, R. A.; Schmid, B. A.; Chemla, D. S. Broadband Terahertz Study of Excitonic Resonances in the High-Density Regime in GaAs− $Al_xGa_{1-x}As$ Quantum Wells. *Phys. Rev. B: Condens. Matter Mater. Phys.* **2005**, *72*, 161314.
(31) Kaindl, R. A.; Hägele, D.; Carnahan, M. A.; Chemla, D. S. Transient Terahertz Spectroscopy of Excitons and Unbound Carriers in Quasi-Two-Dimensional Electron-Hole Gases. *Phys. Rev. B: Condens. Matter Mater. Phys.* **2009**, *79*, 45320.
(32) Lloyd-Hughes, J.; Beere, H. E.; Ritchie, D. A.; Johnston, M. B. Terahertz Magnetoconductivity of Excitons and Electrons in Quantum Cascade Structures. *Phys. Rev. B: Condens. Matter Mater. Phys.* **2008**, *77*, 125322.
(33) Talbert, E. M.; Zarick, H. F.; Boulesbaa, A.; Soetan, N.; Puretzky, A. A.; Geohegan, D. B.; Bardhan, R. Bromine Substitution Improves Excited-State Dynamics in Mesoporous Mixed Halide Perovskite Films. *Nanoscale* **2017**, *9*, 12005−12013.
(34) Frost, J. M. Calculating Polaron Mobility in Halide Perovskites. *Phys. Rev. B: Condens. Matter Mater. Phys.* **2017**, *96*, 195202.
(35) Yu, P. Y.; Cardona, M. *Fundamentals of Semiconductors: Physics and Materials Properties*; Springer Science and Business Media, 2010.
(36) Fröhlich, H. Electrons in Lattice Fields. *Adv. Phys.* **1954**, *3*, 325−361.
(37) Milot, R. L.; Eperon, G. E.; Snaith, H. J.; Johnston, M. B.; Herz, L. M. Temperature-Dependent Charge-Carrier Dynamics in $CH_3NH_3PbI_3$ Perovskite Thin Films. *Adv. Funct. Mater.* **2015**, *25*, 6218−6227.
(38) Savenije, T. J.; Ponseca, C. S.; Kunneman, L.; Abdellah, M.; Zheng, K.; Tian, Y.; Zhu, Q.; Canton, S. E.; Scheblykin, I. G.; Pullerits, T.; et al. Thermally Activated Exciton Dissociation and Recombination Control the Carrier Dynamics in Organometal Halide Perovskite. *J. Phys. Chem. Lett.* **2014**, *5*, 2189−2194.
(39) Karakus, M.; Jensen, S. A.; D'Angelo, F.; Turchinovich, D.; Bonn, M.; Canovas, E. Phonon-Electron Scattering Limits Free Charge Mobility in Methylammonium Lead Iodide Perovskites. *J. Phys. Chem. Lett.* **2015**, *6*, 4991−4996.
(40) Lee, H.-W. Matrix Elements and Cross Section of Raman Scattering by Atomic Hydrogen. *Publications of The Korean Astronomical Society* **2007**, *22*, 21−33.
(41) Kampfrath, T.; Battiato, M.; Maldonado, P.; Eilers, G.; Nötzold, J.; Mährlein, S.; Zbarsky, V.; Freimuth, F.; Mokrousov, Y.; Blügel, S.; et al. Terahertz Spin Current Pulses Controlled by Magnetic Heterostructures. *Nat. Nanotechnol.* **2013**, *8*, 256.
(42) Seifert, T.; Jaiswal, S.; Sajadi, M.; Jakob, G.; Winnerl, S.; Wolf, M.; Kläui, M.; Kampfrath, T. Ultrabroadband single-cycle terahertz pulses with peak fields of 300 kV cm1 from a metallic spintronic emitter. *Appl. Phys. Lett.* **2017**, *110*, 252402.
(43) Seifert, T.; Jaiswal, S.; Martens, U.; Hannegan, J.; Braun, L.; Maldonado, P.; Freimuth, F.; Kronenberg, A.; Henrizi, J.; Radu, I.; et al. Efficient Metallic Spintronic Emitters of Ultrabroadband Terahertz Radiation. *Nat. Photonics* **2016**, *10*, 483.
(44) Klingshirn, C. F. *Semiconductor Optics*, 1st ed.; Springer, 1997; p 166.
(45) Joyce, H. J.; Docherty, C. J.; Gao, Q.; Tan, H. H.; Jagadish, C.; Lloyd-Hughes, J.; Herz, L. M.; Johnston, M. B. Electronic Properties of GaAs, InAs and InP Nanowires Studied by Terahertz Spectroscopy. *Nanotechnology* **2013**, *24*, 214006.

DOI: 10.1021/acs.jpclett.8b01628
J. Phys. Chem. Lett. 2018, 9, 4502−4511

(46) Lloyd-Hughes, J.; Jeon, T.-I. A Review of the Terahertz Conductivity of Bulk and Nano-Materials. *J. Infrared, Millimeter, Terahertz Waves* **2012**, *33*, 871−9252.
(47) Joyce, H. J.; Boland, J. L.; Davies, C. L.; Baig, S. A.; Johnston, M. B. A Review of the Electrical Properties of Semiconductor Nanowires: Insights Gained From Terahertz Conductivity Spectroscopy. *Semicond. Sci. Technol.* **2016**, *31*, 103003.
(48) Fang, H.-H.; Wang, F.; Adjokatse, S.; Zhao, N.; Even, J.; Antonietta Loi, M. Photoexcitation Dynamics in Solution-Processed Formamidinium Lead Iodide Perovskite Thin Films for Solar Cell Applications. *Light: Sci. Appl.* **2016**, *5*, e16056.
(49) Fang, H.-H.; et al. Exciton Recombination in Formamidinium Lead Triiodide: Nanocrystals versus Thin Films. *Small* **2017**, *13*, 1700673.
(50) Galkowski, K.; Mitioglu, A.; Miyata, A.; Plochocka, P.; Portugall, O.; Eperon, G. E.; Wang, J. T.-W.; Stergiopoulos, T.; Stranks, S. D.; Snaith, H. J.; et al. Determination of the Exciton Binding Energy and Effective Masses for Methylammonium and Formamidinium Lead Tri-Halide Perovskite Semiconductors. *Energy Environ. Sci.* **2016**, *9*, 962−970.
(51) Makado, P. C.; McGill, N. C. Energy Levels of a Neutral Hydrogen-Like System in a Constant Magnetic Field of Arbitrary Strength. *J. Phys. C: Solid State Phys.* **1986**, *19*, 873.
(52) Aldrich, C.; Greene, R. L. Hydrogen-Like Systems in Arbitrary Magnetic Fields A Variational Approch. *Phys. Status Solidi B* **1979**, *93*, 343−350.
(53) Stoumpos, C. C.; Malliakas, C. D.; Kanatzidis, M. G. Semiconducting Tin and Lead Iodide Perovskites with Organic Cations: Phase Transitions, High Mobilities, and Near-Infrared Photoluminescent Properties. *Inorg. Chem.* **2013**, *52*, 9019−9038.
(54) Weller, M. T.; Weber, O. J.; Frost, J. M.; Walsh, A. Cubic Perovskite Structure of Black Formamidinium Lead Iodide, α-$[HC(NH_2)_2]PbI_3$, at 298 K. *J. Phys. Chem. Lett.* **2015**, *6*, 3209−3212.
(55) Fabini, D. H.; Stoumpos, C. C.; Laurita, G.; Kaltzoglou, A.; Kontos, A. G.; Falaras, P.; Kanatzidis, M. G.; Seshadri, R. Reentrant Structural and Optical Properties and Large Positive Thermal Expansion in Perovskite Formamidinium Lead Iodide. *Angew. Chem., Int. Ed.* **2016**, *55*, 15392−15396.
(56) Chen, T.; Foley, B. J.; Park, C.; Brown, C. M.; Harriger, L. W.; Lee, J.; Ruff, J.; Yoon, M.; Choi, J. J.; Lee, S.-H. Entropy-Driven Structural Transition and Kinetic Trapping in Formamidinium Lead Iodide Perovskite. *Science advances* **2016**, *2*, e1601650.
(57) Chen, T.; Chen, W.-L.; Foley, B. J.; Lee, J.; Ruff, J. P. C.; Ko, J. Y. P.; Brown, C. M.; Harriger, L. W.; Zhang, D.; Park, C.; et al. Origin of Long Lifetime of Band-Edge Charge Carriers in OrganicInorganic Lead Iodide Perovskites. *Proc. Natl. Acad. Sci. U. S. A.* **2017**, *114*, 7519−7524.
(58) Baikie, T.; Fang, Y.; Kadro, J. M.; Schreyer, M.; Wei, F.; Mhaisalkar, S. G.; Grätzel, M.; White, T. J. Synthesis and Crystal Chemistry of the Hybrid Perovskite $(CH_3NH_3PbI_3)$ for Solid-State Sensitized Solar Applications. *J. Mater. Chem. A* **2013**, *1*, 5628.
(59) Protesescu, L.; Yakunin, S.; Kumar, S.; Bär, J.; Bertolotti, F.; Masciocchi, N.; Guagliardi, A.; Grotevent, M.; Shorubalko, I.; Bodnarchuk, M. I.; et al. Dismantling the Red Wall of Colloidal Perovskites: Highly Luminescent Formamidinium and FormamidiniumCesium Lead Iodide Nanocrystals. *ACS Nano* **2017**, *11*, 3119−3134.
(60) Fabini, D. H.; Siaw, T. A.; Stoumpos, C. C.; Laurita, G.; Olds, D.; Page, K.; Hu, J. G.; Kanatzidis, M. G.; Han, S.; Seshadri, R. Universal Dynamics of Molecular Reorientation in Hybrid Lead Iodide Perovskites. *J. Am. Chem. Soc.* **2017**, *139*, 16875−16884.
(61) Carignano, M. A.; Saeed, Y.; Aravindh, S. A.; Roqan, I. S.; Even, J.; Katan, C. A Close Examination of the Structure and Dynamics of $HC(NH_2)_2PbI_3$ by MD Simulations and Group Theory. *Phys. Chem. Chem. Phys.* **2016**, *18*, 27109−27118.
(62) Wasylishen, R. E.; Knop, O.; Macdonald, J. B. Cation Rotation in Methylammonium Lead Halides. *Solid State Commun.* **1985**, *56*, 581−582.
(63) Fabini, D. H.; Hogan, T.; Evans, H. A.; Stoumpos, C. C.; Kanatzidis, M. G.; Seshadri, R. Dielectric and Thermodynamic Signatures of Low-Temperature Glassy Dynamics in the Hybrid Perovskites $CH_3NH_3PbI_3$ and $HC(NH_2)_2PbI_3$. *J. Phys. Chem. Lett.* **2016**, *7*, 376−381.
(64) Gélvez-Rueda, M. C.; Renaud, N.; Grozema, F. C. Temperature Dependent Charge Carrier Dynamics in Formamidinium Lead Iodide Perovskite. *J. Phys. Chem. C* **2017**, *121*, 23392−23397.
(65) Frost, J. M.; Butler, K. T.; Brivio, F.; Hendon, C. H.; Van Schilfgaarde, M.; Walsh, A. Atomistic Origins of High-Performance in Hybrid Halide Perovskite Solar Cells. *Nano Lett.* **2014**, *14*, 2584−2590.
(66) Varshni, Y. P. Temperature Dependence of the Energy Gap in Semiconductors. *Physica* **1967**, *34*, 149−154.
(67) Sestu, N.; Cadelano, M.; Sarritzu, V.; Chen, F.; Marongiu, D.; Piras, R.; Mainas, M.; Quochi, F.; Saba, M.; Mura, A.; et al. Absorption F-Sum Rule for the Exciton Binding Energy in Methylammonium Lead Halide Perovskites. *J. Phys. Chem. Lett.* **2015**, *6*, 4566−4572.
(68) Yang, Y.; Ostrowski, D. P.; France, R. M.; Zhu, K.; Van De Lagemaat, J.; Luther, J. M.; Beard, M. C. Observation of a Hot-Phonon Bottleneck in Lead-Iodide Perovskites. *Nat. Photonics* **2016**, *10*, 53−59.
(69) Hellwarth, R. W.; Biaggio, I. Mobility of an Electron in a Multimode Polar Lattice. *Phys. Rev. B: Condens. Matter Mater. Phys.* **1999**, *60*, 299−307.
(70) Wehrenfennig, C.; Liu, M.; Snaith, H. J.; Johnston, M. B.; Herz, L. M. Charge Carrier Recombination Channels in the Low-Temperature Phase of Organic-Inorganic Lead Halide Perovskite Thin Films. *APL Mater.* **2014**, *2*, 081513.

DOI: 10.1021/acs.jpclett.8b01628
J. Phys. Chem. Lett. 2018, 9, 4502−4511